

Constitutive modelling of PMMA-based bone cement: a functional model of viscoelasticity and its approximation for time domain investigations

A. LION¹⁾, B. YAGIMLI¹⁾, G. BAROUD²⁾, U. GOERKE³⁾

¹⁾*Institute of Mechanics
Department of Aerospace Engineering
University of the Federal Armed Forces Munich
D-85577 Neubiberg, Germany*

²⁾*Department of Mechanical Engineering
Biomechanics Laboratory
University of Sherbrooke
Quebec, Canada J1K 2R1*

³⁾*Department of Mechanical Engineering
Institute of Mechanics and Thermodynamics
Technical University of Chemnitz
Straße der Nationen 62, 09111 Chemnitz, Germany*

TO REPRESENT THE MECHANICAL BEHAVIOUR of polyethylmethacrylate-based bone cement, a constitutive approach of finite linear viscoelasticity is formulated and identified. Motivated by the experimental data of storage and loss modulus, the model is based on a three-dimensional functional in integral representation. In the investigated frequency range, the master curve of the loss modulus is constant and that of the storage modulus increases linearly with the logarithm of the frequency. This behaviour corresponds to a viscoelastic fluid, and can be described by a continuous relaxation spectrum. For numerical simulations which are planned in future, the constitutive functional is approximated by a discrete spectrum. To this end, an earlier-developed method to approximate continuous relaxation spectra in limited time or frequency ranges by discrete ones is applied.

Notations

$\varepsilon, \varepsilon_0, \Delta\varepsilon, \lambda, \lambda_0$ strain, static strain, strain amplitude, stretch, static stretch,
 σ, σ_0 stress, mean stress,
 a_k, b_k Fourier coefficients,
 f, ω, T frequency, angular frequency, duration of a loading cycle,
 $\theta, \theta_0, a(\theta)$ temperature, reference temperature, shift function,
F, L, D deformation gradient, velocity gradient, strain rate tensor,
C, B, e left and right Cauchy Green tensor, Piola strain tensor,

$\mathbf{F}_0, \mathbf{f}(t)$	static and time-dependent parts of the deformation gradient,
$\mathbf{h}(t)$	incremental displacement gradient,
\mathbf{E}_L	infinitesimal strain tensor,
$\mathbf{C}_0, \mathbf{e}_0$	static left Cauchy Green and Piola strain tensor,
$\mathbf{1}, p$	unit tensor of the second order, hydrostatic pressure,
\mathbf{T}, \mathbf{S}	Cauchy stress tensor, deviatoric stress tensor,
$\tilde{\mathbf{T}}, \tilde{\mathbf{S}}$	stress tensors of the 2nd Piola Kirchhoff type,
μ, z, η	material parameters of a Maxwell element,
$\mu_0, z_{\min}, z_{\max}$	material parameters of the hyperbola-type relaxation spectrum,
I, II, III	invariants of a second order tensor,
$\text{tr}(\bullet), \det(\bullet)$	trace and determinant operators,
G', G'', G^*	storage modulus, loss modulus, complex modulus,
$G(t), h(z), \Gamma(\nu)$	relaxation function, relaxation spectrum, cumulative spectrum,
G_0, G_k, ν_k, N	material parameters of the Prony series,
ν_{\min}, ν_{\max}	smallest and largest relaxation frequencies in the Prony series,
τ_{\min}, τ_{\max}	limits of the time range of interest.

1. Introduction

IN THE PRESENT PAPER, a constitutive approach is developed in order to model the viscoelastic behaviour of polymerized PMMA-based bone cement. The model can be used to represent the long- and short-term behaviour of the polymerized cement under mechanical loads, but the polymerization process is not taken into account. Readers who are interested in this topic are referred to the comprehensive article of STANCZYK [21]. The investigated PMMA specimens were cured at room temperature under ambient atmosphere conditions and the mechanical experiments were carried out in an air-conditioned laboratory; its relative air moisture was about 50%. Thus, the influence of the humid and saline environment of the human body is not taken into account. For stiffness and strength investigations of bone cement stored in a salty Ringer solution the reader is referred, for example, to HARPER *et al.* [8].

The paper starts with an introduction, where some background information about bone cement and its medical application is provided. In the experimental section, our tests to determine the inelastic material properties are described, evaluated and interpreted. In the modelling section, the general constitutive approach of finite linear viscoelasticity is formulated, specialized and identified. It is based on a continuous relaxation time distribution and contains only three material parameters. Since viscoelasticity models of this type can not easily be implemented into commercial finite element codes, an approximation technique in terms of discrete spectra is applied. The paper concludes with a discussion.

To fix metallic endoprostheses, polymethylmethacrylate- or PMMA-based bone cement is successfully applied for many years. A recent application in the

context of minimal invasive surgery is the reinforcement of osteoporotic vertebrae with PMMA cement or, alternatively, with biocement (cf. DOROZHKIN [7]). The infiltration of osteoporotic vertebrae with cement leads to a stabilization of the bone and prevents osteoporotic vertebral fractures (see BAROUD *et al.* [1]). As it is well known, there are two different medical techniques which are known as kyphoplasty and vertebroplasty. In vertebroplasty, the fluid cement is directly injected into the osteoporotic bone. But in kyphoplasty, it is injected into a hole in the bone which has been formed with an inflated rubber balloon. For more details concerning these methods, we refer the reader to the essays of BAROUD *et al.* [1, 2, 4], HEINI *et al.* [12] and ROHLMANN *et al.* [19, 20]. The polymerization of PMMA-based bone cement is exothermal (see STANCZYK [21] and citations therein or MAZZULLO *et al.* [18]) and is accompanied by a shrinkage in volume of about 5%. As a consequence of the exothermal heating in combination with the shrinkage as well as due to the difference in the thermal expansion behaviour of human bone and bone cement, residual stresses evolve with time. Since both the curing and the cured cement are viscoelastic materials, time-dependent changes in the local stress distribution due to creep and relaxation also occur (cf. BAROUD and VANT [3] or VERDONSHOT and HUISKES [23]). The important question whether the residual stresses decay completely or not after the polymerization, can only be answered if both the thermomechanical and the chemical material properties of both the curing and the cured cement are known. A thermomechanical chemical constitutive model to describe such effects has been proposed by LION and HÖFER [17]. The experimental parameter identification is currently in progress. Damage effects in PMMA due to long-term creep loadings have also been observed (cf. KIM *et al.* [12] or LENNON and PRENDERGAST [14]).

Since the Young modulus of PMMA under short time loads is about 10–12 times larger than that of a typical bone, local load shifts on the intervertebral discs can occur (see BAROUD *et al.* [1] and HEINI *et al.* [12]). In order to study all these phenomena, numerical simulations with appropriate constitutive models are extremely helpful. In this context, BAROUD *et al.* [1] have estimated the stress distribution in the intervertebral disc with finite element simulations of non-reinforced and reinforced vertebra systems. These simulations were carried out on the basis of the assumption that the cement is an isotropic linear-elastic material. This hypothesis does not take the viscoelastic material behaviour into account but forms a good foundation for estimations and short-term simulations.

In order to estimate the time-dependent degree of cure and temperature distributions during the polymerization in PMMA-reinforced bones, STANCZYK [21] developed a physically-based model (see also LI *et al.* [15]). To the knowledge of the authors, there are at present no holistic constitutive models and numerical simulations which take all important effects into account: polymerization, exothermal heat generation, chemical shrinking, thermal expansion, phase tran-

sition of PMMA from a viscous fluid to a thermoviscoelastic solid, evolution of residual stresses.

As the very first step, it is the aim of this work to develop and identify a constitutive model of viscoelasticity that is able to represent the isothermal mechanical behaviour of PMMA-based bone cement. With such a model in combination with the finite element method, it is possible to simulate time-dependent stresses and deformations in PMMA-reinforced bones. In the experimental part of this essay, the material behaviour of the PMMA cement is investigated using the technique of dynamical mechanical analysis (DMA). Based on the data of storage and loss modulus, a constitutive model of viscoelasticity in functional formulation is applied and a continuous relaxation spectrum of truncated hyperbola type, as proposed by TOBOLSKY [22], is identified. Models of this type are investigated in a more general thermodynamic framework by HAUPT and LION [11]. In order to obtain a formulation of the proposed stress functional in terms of ordinary differential equations which can easily be implemented into finite element codes, the approximation technique developed by HAUPT *et al.* [10] is applied. The implementation as well as the extension of this approach to cover the exothermal curing behaviour is the aim of a current research project.

2. Experiments

To study the material properties of the bone cement, the dynamic mechanical analysis (DMA) testing machine GABO Eplexor 500 as shown in Fig. 1 was used. Sinusoidal displacement- or force-controlled excitations can be prescribed and the corresponding response of the material is recorded. The frequency range is between 0.01 Hz and 100 Hz, the temperature range is between -150°C and 500°C , the maximum force amplitude is 500 N and the maximum total force is 1500 N.

The PMMA specimens were cured at room temperature under ambient atmosphere conditions and the dynamic mechanical analyses were carried out in an air-conditioned laboratory with a relative air moisture of 50%. For the sample preparation, the PMMA cement DP-pour without any X-ray contrast agent and medical additive was used. It was produced by the DenPlus Inc. in Canada. After mixing the polymer powder and the fluid monomer, the homogeneous mixture was filled into a casting mould having the shape of a dog-bone. Then, the specimens were cured at room temperature under laboratory conditions and removed from the mould. Four weeks after this process, the DMA specimens were cut out from this raw material. They were 40 mm in length, 5 mm in width and 2.5 mm in thickness.

In each experiment, a constant specimen temperature $\theta \in [-40^{\circ}\text{C}, 80^{\circ}\text{C}]$ was prescribed and sampled in 15°C increments. After the thermal equilibrium of the



FIG. 1. Dynamic mechanical analysis system, Eplexor 500, GABO.

specimen was reached, harmonic strains with different frequencies $f = \omega/(2\pi)$, a constant amplitude of $\Delta\varepsilon = 0.002$ and a constant prestrain of $\varepsilon_0 = 0.003$ in the form of

$$(2.1) \quad \varepsilon(t) = \varepsilon_0 + \Delta\varepsilon \sin(2\pi ft)$$

were prescribed. The stationary periodic stress responses were measured and represented as

$$(2.2) \quad \sigma(t) = \sigma_0 + \Delta\varepsilon \sum_{k=1}^{\infty} (a_k \cos(2\pi k ft) + b_k \sin(2\pi k ft)).$$

The mean stress σ_0 and the coefficients a_k and b_k can depend, in principle, on all parameters characterizing the input process, i.e. on $\varepsilon_0, \Delta\varepsilon, f, \theta$.

The coefficients of the Fourier series (2.2) are determined by the formulae

$$a_k = \frac{2}{T} \int_0^T \frac{\sigma(t) - \sigma_0}{\Delta\varepsilon} \cos(2\pi k ft) dt$$

and

$$b_k = \frac{2}{T} \int_0^T \frac{\sigma(t) - \sigma_0}{\Delta\varepsilon} \sin(2\pi k ft) dt.$$

$T = 1/f$ is the duration of a loading cycle. The first coefficients can easily be interpreted as

$$G' = b_1 \quad \text{and} \quad G'' = a_1,$$

where $G'(\omega, \theta, \dots)$ is the storage modulus and $G''(\omega, \theta, \dots)$ the loss modulus.

Since PMMA is reported to behave as a linear viscoelastic material in the investigated stress and temperature range (see BERTILSSON and JANSSON [5]), we applied the known frequency-temperature equivalence principle in order to obtain the master curves for both the storage and the loss modulus (e.g. TOBOLSKY [22]). In this case, the temperature dependence of storage and loss modulus has the form

$$G'(\omega, \theta) = G'(\omega a(\theta), \theta_0) = G'(10^{(\log(\omega) + \log(a(\theta)))}, \theta_0),$$

$$G''(\omega, \theta) = G''(\omega a(\theta), \theta_0) = G''(10^{(\log(\omega) + \log(a(\theta)))}, \theta_0),$$

where θ_0 is an arbitrary reference temperature. The material function $a(\theta) > 0$ is normalized in the sense of $a(\theta_0) = 1$ and has the property $da(\theta)/d\theta \leq 0$ (see, e.g., LION [16]).

Plotting the experimental curves of storage and loss modulus for the different temperatures in a half-logarithmic diagram, taking the choice of a reference temperature and shifting the other curves in horizontal direction just until a smooth master curve is obtained, leads to Fig. 2. For the reference temperature we took

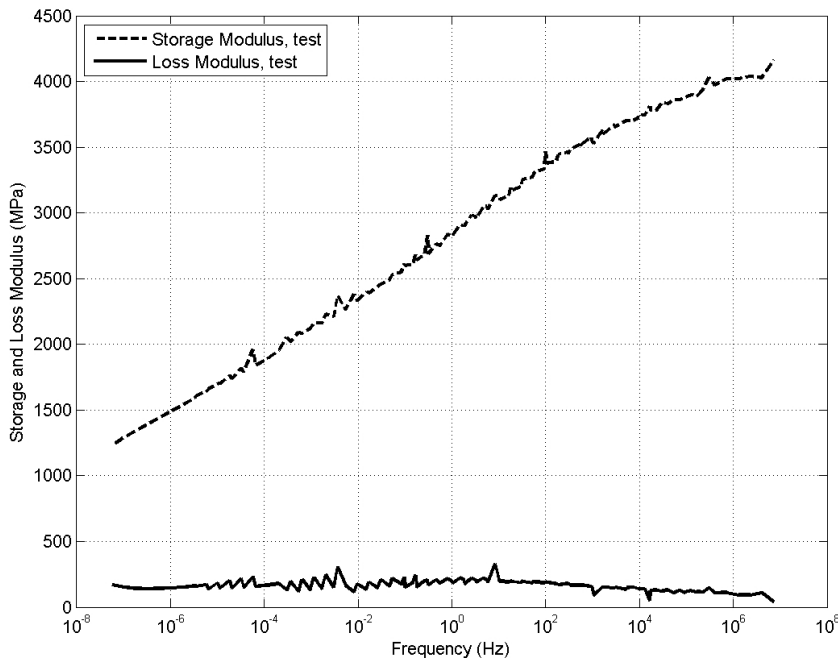


FIG. 2. Experimental data of storage and loss modulus corresponding to $\theta_0 = 293$ K.

the choice of $\theta_0 = 20^\circ\text{C} \approx 293\text{K}$. The figure shows, that the master curve of the loss modulus is nearly constant in the investigated frequency range between 10^{-7} Hz and 10^7 Hz . The master curve of the storage modulus increases linearly with the logarithm of the frequency.

3. Constitutive modelling

In order to represent the material behaviour of the PMMA-based bone cement, we apply the following theory of viscoelasticity. The time-dependent mapping between the position vector $\vec{\mathbf{X}}(P)$ of a material point P of the reference configuration to its position $\vec{\mathbf{x}}(P)$ in the current configuration is described by the vector function $\vec{\mathbf{x}} = \vec{\chi}(\vec{\mathbf{X}}, t)$. On the basis of the deformation gradient

$$\mathbf{F} = \text{Grad}(\vec{\chi}(\vec{\mathbf{X}}, t)),$$

the Right and Left Cauchy Green tensors \mathbf{C} and \mathbf{B} and the Piola strain \mathbf{e} are defined as

$$(3.1) \quad \mathbf{C} = \mathbf{F}^T \mathbf{F}, \quad \mathbf{B} = \mathbf{F} \mathbf{F}^T$$

and

$$(3.2) \quad \mathbf{e} = \frac{1}{2}(\mathbf{C}^{-1} - \mathbf{1}).$$

The velocity gradient \mathbf{L} is written as

$$\mathbf{L} = \dot{\mathbf{F}} \mathbf{F}^{-1}$$

and its symmetric part is the strain rate tensor

$$(3.3) \quad \mathbf{D} = \frac{1}{2}(\mathbf{L} + \mathbf{L}^T).$$

Calculating the material time derivative of the Piola strain tensor, the relation

$$(3.4) \quad \dot{\mathbf{e}} = -\mathbf{F}^{-1} \mathbf{D} \mathbf{F}^{T-1}$$

is obtained. To formulate the model as simple as possible at this early stage, we assume the cement to be incompressible corresponding to $\det(\mathbf{F}) = 1$. Thus, the Cauchy stress tensor \mathbf{T} is the sum of the reaction stress $-p\mathbf{1}$ due to the constraint of incompressibility and the constitutively determined deviatoric stress \mathbf{S} :

$$\mathbf{T} = -p\mathbf{1} + \mathbf{S}.$$

The corresponding stresses of the Second Piola Kirchhoff-type read as

$$(3.5) \quad \tilde{\mathbf{S}} = \mathbf{F}^{-1} \mathbf{S} \mathbf{F}^{T-1}$$

and

$$\tilde{\mathbf{T}} = \mathbf{F}^{-1} \mathbf{T} \mathbf{F}^{T-1}$$

leading to the relation

$$\tilde{\mathbf{T}} = -p \mathbf{C}^{-1} + \tilde{\mathbf{S}}$$

To specify the model for the deviatoric stress \mathbf{S} we formulate a model of finite viscoelasticity which operates without any splitting of the deformation. Its fundament is a Maxwell element in the form of

$$(3.6) \quad \overset{\nabla}{\mathbf{S}} + \frac{1}{z} \mathbf{S} = 2\mu \mathbf{D},$$

where z is the relaxation time and μ is an elasticity constant¹⁾. The expression

$$\overset{\nabla}{\mathbf{S}} = \dot{\mathbf{S}} - \mathbf{L} \mathbf{S} - \mathbf{S} \mathbf{L}^T$$

is an Oldroyd derivative of the deviatoric stress (cf. HAUPT [9] or BÖHME [6]). To solve the differential equation (3.6) for arbitrary deformation processes, we multiply it with the inverse deformation gradient and its transpose

$$\mathbf{F}^{-1} \overset{\nabla}{\mathbf{S}} \mathbf{F}^{T-1} + \frac{1}{z} \mathbf{F}^{-1} \mathbf{S} \mathbf{F}^{T-1} = 2\mu \mathbf{F}^{-1} \mathbf{D} \mathbf{F}^{T-1},$$

and take (3.4) and (3.5) in combination with $\mathbf{F}^{-1} \overset{\nabla}{\mathbf{S}} \mathbf{F}^{T-1} = \overset{\dot{\sim}}{\mathbf{S}}$ into account:

$$\overset{\dot{\sim}}{\mathbf{S}} + \frac{1}{z} \tilde{\mathbf{S}} = -2\mu \dot{\mathbf{e}}.$$

Analytical integration of this differential equation leads to the solution

$$\tilde{\mathbf{S}}(t) = - \int_{-\infty}^t 2\mu e^{-(t-s)/z} \dot{\mathbf{e}}(s) ds,$$

for the stress tensor of the Second Piola Kirchhoff type, or to

$$(3.7) \quad \mathbf{T}(t) = -p \mathbf{1} - \int_{-\infty}^t 2\mu e^{-(t-s)/z} \mathbf{F}(t) \dot{\mathbf{e}}(s) \mathbf{F}^T(t) ds$$

for the Cauchy stress. To interpret the constant μ we assume a deformation process whose duration is essentially shorter than the relaxation time z . Then, the approximation $e^{-(t-s)/z} \approx 1$ holds which yields

$$\mathbf{T}(t) = -p \mathbf{1} - 2\mu \int_{-\infty}^t \mathbf{F}(t) \dot{\mathbf{e}}(s) \mathbf{F}^T(t) ds$$

¹⁾As an alternative frequently used in fluid mechanics, some authors introduce the viscosity $\eta/z = \mu$ on the right-hand side of (3.6).

or after integration together with the assumption $\mathbf{e}(-\infty) = \mathbf{0}$

$$\mathbf{T}(t) = -p\mathbf{1} - 2\mu\mathbf{F}(t)\mathbf{e}(t)\mathbf{F}^T(t).$$

An elementary calculation together with the definitions (3.1) and (3.2) leads to

$$\mathbf{T}(t) = -p\mathbf{1} + \mu(\mathbf{B}(t) - \mathbf{1}) = -\bar{p}\mathbf{1} + \mu\mathbf{B}(t),$$

which is the Neo–Hookean model of finite elasticity. If, on the other hand, the relaxation time z is short in comparison with a typical time constant characterizing the deformation process, we use a reformulation of (3.6):

$$\overset{\nabla}{\mathbf{S}} + \frac{1}{z}\mathbf{S} = 2\frac{\eta}{z}\mathbf{D}.$$

If z is sufficiently small, the stress rate term can be neglected such that the equation $\mathbf{S} = 2\eta\mathbf{D}$ or $\mathbf{T} = -p\mathbf{1} + 2\eta\mathbf{D}$ of an incompressible Navier–Stokes fluid is obtained.

Since the time-dependent relaxation behaviour of PMMA cannot be described quantitatively with one single exponential function, we introduce the generalisation

$$(3.8) \quad \mathbf{T}(t) = -p\mathbf{1} - 2 \int_{-\infty}^t G(t-s)\mathbf{F}(t)\dot{\mathbf{e}}(s)\mathbf{F}^T(t)ds$$

of (3.7), where the relaxation function is a continuous distribution of exponentials:

$$(3.9) \quad G(t) = \int_0^{\infty} h(z)e^{-t/z}dz, \quad h \geq 0.$$

HAUPT and LION [11] have shown that the model (3.8) is compatible with the second law of thermodynamics when the relaxation function satisfies

$$G(t) \geq 0, \quad G'(t) \leq 0, \quad G''(t) \geq 0.$$

Since $h \geq 0$ in (3.9), this requirement is satisfied.

3.1. Linearization of the constitutive model

In order to identify the material parameters of the model defined by (3.8) and (3.9), uniaxial dynamic mechanical analyses under tension/compression were performed; the strain is given by (2.1). To describe excitations of this type

in three dimensions, the deformation gradient is multiplicatively decomposed into a time-independent predeformation \mathbf{F}_0 and a time-dependent part $\mathbf{f}(t)$:

$$(3.10) \quad \mathbf{F}(t) = \mathbf{f}(t)\mathbf{F}_0.$$

This time-dependent part is represented as the sum of a unit tensor and an incremental displacement gradient

$$(3.11) \quad \mathbf{f}(t) = \mathbf{1} + \mathbf{h}(t),$$

whose magnitude

$$\delta = \max_{\substack{\vec{\mathbf{X}} \in \text{material body} \\ -\infty \leq t < \infty}} (\|\mathbf{h}(\vec{\mathbf{X}}, t)\|) \leq 1$$

is assumed to be sufficiently small. Under this assumption, the inverse Right Cauchy–Green tensor $\mathbf{C}^{-1} = \mathbf{F}^{-1}\mathbf{F}^{T-1}$ and, as a consequence, the Piola tensor defined in (3.2) can be linearized:

$$\mathbf{C}^{-1} = ((\mathbf{1} + \mathbf{h})\mathbf{F}_0)^{-1}((\mathbf{1} + \mathbf{h})\mathbf{F}_0)^{T-1} = \mathbf{F}_0^{-1}(\mathbf{1} + \mathbf{h})^{-1}(\mathbf{1} + \mathbf{h})^{T-1}\mathbf{F}_0^{T-1}.$$

Using the Cayley–Hamilton equation (cf. HAUPT [9])

$$(\mathbf{1} + \mathbf{h})^{-1} = \frac{1}{III_{\mathbf{1}+\mathbf{h}}}((\mathbf{1} + \mathbf{h})^2 - I_{\mathbf{1}+\mathbf{h}}(\mathbf{1} + \mathbf{h}) + II_{\mathbf{1}+\mathbf{h}}\mathbf{1})$$

together with the definitions and linearized forms of the invariants of the tensor $\mathbf{1} + \mathbf{h}$,

$$I_{\mathbf{1}+\mathbf{h}} = \text{tr}(\mathbf{1} + \mathbf{h}) = 3 + I_{\mathbf{h}},$$

$$II_{\mathbf{1}+\mathbf{h}} = \frac{1}{2}(I_{\mathbf{1}+\mathbf{h}}^2 - \text{tr}((\mathbf{1} + \mathbf{h})^2)) = 3 + 2I_{\mathbf{h}} + O(\delta^2),$$

$$III_{\mathbf{1}+\mathbf{h}} = \det(\mathbf{1} + \mathbf{h}) = 1 + I_{\mathbf{h}} + O(\delta^2),$$

the linearization

$$(\mathbf{1} + \mathbf{h})^{-1} = \mathbf{1} - \mathbf{h} + O(\delta^2)$$

is obtained²⁾. Considering this result, we obtain

$$\mathbf{C}^{-1} = (\mathbf{F}_0^{-1}(\mathbf{1} - \mathbf{h}))((\mathbf{1} - \mathbf{h}^T)\mathbf{F}_0^{T-1}) + O(\delta^2)$$

or, after rearranging terms,

$$(3.12) \quad \mathbf{C}^{-1} = \mathbf{F}_0^{-1}\mathbf{F}_0^{T-1} - 2\mathbf{F}_0^{-1}\left(\frac{1}{2}(\mathbf{h} + \mathbf{h}^T)\right)\mathbf{F}_0^{T-1} + O(\delta^2).$$

²⁾The formulation $f(x) = O(x^n)$ means that $|f(x)|/x^n \rightarrow C$ for $x \rightarrow 0$ (Landau's symbol).

With the definition of the infinitesimal strain tensor as the symmetric part of the incremental displacement gradient,

$$\mathbf{E}_L = \frac{1}{2}(\mathbf{h} + \mathbf{h}^T),$$

(3.12) leads to the linearization of the inverse Right Cauchy–Green tensor

$$\mathbf{C}^{-1} = \mathbf{C}_0^{-1} - 2\mathbf{F}_0^{-1}\mathbf{E}_L\mathbf{F}_0^{T-1} + O(\delta^2)$$

and to that of the Piola strain tensor

$$\mathbf{e} = \mathbf{e}_0 - \mathbf{F}_0^{-1}\mathbf{E}_L\mathbf{F}_0^{T-1} + O(\delta^2)$$

Inserting this expression in combination with (3.10) and (3.11) into the stress functional (3.8),

$$\mathbf{T}(t) = -p\mathbf{1} - 2 \int_{-\infty}^t G(t-s)(\mathbf{1} + \mathbf{h}(t))\mathbf{F}_0(\mathbf{F}_0^{-1}\dot{\mathbf{E}}_L(s)\mathbf{F}_0^{T-1})\mathbf{F}_0^T(\mathbf{1} + \mathbf{h}^T(t))ds + O(\delta^2),$$

the linearized version of the constitutive model is obtained:

$$(3.13) \quad \mathbf{T}(t) = -p\mathbf{1} + 2 \int_{-\infty}^t G(t-s)\dot{\mathbf{E}}_L(s)ds + O(\delta^2).$$

As we see, the Cauchy stress tensor which acts on the current configuration is independent of the static deformation \mathbf{F}_0 .

3.2. Calculation of dynamic moduli

In order to calculate the dynamic moduli G' and G'' we assume $\lambda = \lambda(t)$, $\lambda_0 = \text{const}$ and prescribe the deformation gradient and its static part as

$$\begin{aligned} \mathbf{F} &= \lambda \vec{\mathbf{e}}_1 \otimes \vec{\mathbf{e}}_1 + \lambda^{-1/2}(\vec{\mathbf{e}}_2 \otimes \vec{\mathbf{e}}_2 + \vec{\mathbf{e}}_3 \otimes \vec{\mathbf{e}}_3), \\ \mathbf{F}_0 &= \lambda_0 \vec{\mathbf{e}}_1 \otimes \vec{\mathbf{e}}_1 + \lambda_0^{-1/2}(\vec{\mathbf{e}}_2 \otimes \vec{\mathbf{e}}_2 + \vec{\mathbf{e}}_3 \otimes \vec{\mathbf{e}}_3) \end{aligned}$$

leading to

$$\mathbf{h}(t) = \mathbf{F}(t)\mathbf{F}_0^{-1} - \mathbf{1}$$

or

$$(3.14) \quad \mathbf{h} = \left(\frac{\lambda}{\lambda_0} - 1\right) \vec{\mathbf{e}}_1 \otimes \vec{\mathbf{e}}_1 + \left(\left(\frac{\lambda_0}{\lambda}\right)^{1/2} - 1\right)(\vec{\mathbf{e}}_2 \otimes \vec{\mathbf{e}}_2 + \vec{\mathbf{e}}_3 \otimes \vec{\mathbf{e}}_3).$$

The initial length of the virgin specimen is L_R , the length of the statically deformed specimen is L_0 and the current length is L . Then, we obtain $\lambda_0 = L_0/L_R$ and $\lambda = L/L_R$ which leads to $\lambda/\lambda_0 = L/L_0 = (L_0 + \Delta L)/L_0 = 1 + \varepsilon$ if the

change in length $\Delta L(t)$ is related to the length of the predeformed specimen, i.e. $\varepsilon(t) = \Delta L/L_0$. Linearization of (3.14) for $|\varepsilon| \ll 1$ leads to

$$\mathbf{h} = \varepsilon(t)\vec{\mathbf{e}}_1 \otimes \vec{\mathbf{e}}_1 - \frac{1}{2}\varepsilon(t)(\vec{\mathbf{e}}_2 \otimes \vec{\mathbf{e}}_2 + \vec{\mathbf{e}}_3 \otimes \vec{\mathbf{e}}_3)$$

for the incremental displacement gradient and for the infinitesimal strain tensor to

$$(3.15) \quad \mathbf{E}_L = \varepsilon(t)\vec{\mathbf{e}}_1 \otimes \vec{\mathbf{e}}_1 - \frac{1}{2}\varepsilon(t)(\vec{\mathbf{e}}_2 \otimes \vec{\mathbf{e}}_2 + \vec{\mathbf{e}}_3 \otimes \vec{\mathbf{e}}_3)$$

with

$$(3.16) \quad \varepsilon(t) = \Delta\varepsilon \sin(2\pi ft).$$

Taking (3.13), (3.15) and (3.16) and into account and assuming a uniaxial state of stress

$$\mathbf{T} = \sigma(t)\vec{\mathbf{e}}_1 \otimes \vec{\mathbf{e}}_1,$$

leads to the scalar equations

$$\sigma(t) = -p + 2 \int_{-\infty}^t G(t-s)\dot{\varepsilon}(s)ds \quad \text{and} \quad 0 = -p - \int_{-\infty}^t G(t-s)\dot{\varepsilon}(s)ds$$

or to the uniaxial stress strain functional

$$\sigma(t) = 3 \int_{-\infty}^t G(t-s)\dot{\varepsilon}(s)ds$$

after eliminating the constitutively undetermined pressure. To derive the storage and the loss modulus, we prescribe $\varepsilon(t) = \hat{\varepsilon}e^{i\omega t}$ and $\sigma(t) = \hat{\sigma}e^{i\omega t}$ for stress and strain³⁾ and obtain

$$\hat{\sigma}e^{i\omega t} = 3i\omega\hat{\varepsilon} \int_{-\infty}^t G(t-s)e^{i\omega s}ds = \left(3i\omega\hat{\varepsilon} \int_0^{\infty} G(s)e^{-i\omega s}ds\right)e^{i\omega t}.$$

Corresponding to the relation $\hat{\sigma} = G^*(\omega)\hat{\varepsilon}$, the complex modulus reads as

$$(3.17) \quad G^*(\omega) = 3i\omega \int_0^{\infty} G(s)e^{-i\omega s}ds.$$

³⁾ $i = \sqrt{-1}$ is the imaginary unit.

Inserting the spectral representation (3.9) of the relaxation function $G(t)$ into (3.17) and interchanging the sequence of integration, leads to the intermediate result

$$G^*(\omega) = 3i\omega \int_0^\infty \left(\int_0^\infty h(z) e^{-\frac{s}{z}} dz \right) e^{-i\omega s} ds = 3i\omega \int_0^\infty h(z) \left(\int_0^\infty e^{-(i\omega + 1/z)s} ds \right) dz.$$

Carrying out the integration with respect to the variable s , the relation

$$(3.18) \quad G^*(\omega) = 3 \int_0^\infty h(z) \frac{i\omega z}{1 + i\omega z} dz = 3 \int_0^\infty h(z) \frac{(\omega z)^2 + i\omega z}{1 + (\omega z)^2} dz$$

is obtained. Splitting (3.18) into real and imaginary parts leads finally to

$$(3.19) \quad G'(\omega) = \text{Re}(G^*) = 3 \int_0^\infty h(z) \frac{(\omega z)^2}{1 + (\omega z)^2} dz$$

for the storage modulus and to

$$(3.20) \quad G''(\omega) = \text{Im}(G^*) = 3 \int_0^\infty h(z) \frac{\omega z}{1 + (\omega z)^2} dz$$

for the loss modulus. To represent the experimental data of the storage and loss modulus, we consider the relaxation spectrum of hyperbola type⁴⁾

$$(3.21) \quad h(z) = \begin{cases} \frac{\mu_0}{z} & \text{if } z_{\min} \leq z \leq z_{\max}, \\ 0 & \text{else,} \end{cases}$$

proposed by TOBOLSKY [22], insert it into (3.19) and (3.20),

$$G'(\omega) = 3\mu_0 \int_{z_{\min}}^{z_{\max}} \frac{(\omega z)^2}{1 + (\omega z)^2} dz, \quad G''(\omega) = 3\mu_0 \int_{z_{\min}}^{z_{\max}} \frac{\omega z}{1 + (\omega z)^2} dz$$

and obtain the final relation

$$(3.22) \quad G'(\omega) = \frac{3\mu_0}{2} \ln \left(\frac{1 + (\omega z_{\max})^2}{1 + (\omega z_{\min})^2} \right)$$

for the storage modulus and

$$(3.23) \quad G''(\omega) = 3\mu_0 (\text{arctg}(\omega z_{\max}) - \text{arctg}(\omega z_{\min}))$$

⁴⁾The material parameters z_{\min} and z_{\max} are the smallest and largest relaxation times of the material and the constant μ_0 has the meaning of an elastic modulus (but is not the Young modulus).

for the loss modulus. The constants z_{\min} and z_{\max} are the smallest and largest relaxation times of the material and μ_0 is a modulus.

In the case of $\omega z_{\min} \ll 1$ and $\omega z_{\max} \gg 1$, (3.22) and (3.23) lead to a storage modulus which is proportional to the logarithm of the frequency $G'(\omega) \approx 3\mu_0 \ln(\omega z_{\max})$ and to a loss modulus $G''(\omega) \approx 3\mu_0$ which is independent of the frequency. This behaviour has been observed in the experiments.

3.3. Estimation of the material parameters

The plateau, where the loss modulus is nearly constant, can be used to identify the constant μ_0 and the linear behaviour of the storage modulus can be used to determine z_{\max} . Thus, from the available experimental data the smallest relaxation time z_{\min} cannot be estimated with high accuracy.

Table 1. Material parameters of PMMA-based bone cement.

z_{\max}	z_{\min}	μ_0
10^{12} sec	10^{-7} sec	32.3 MPa

The identification of the material parameters leads to the values listed in Table 1. The quality of the fit is shown in Fig. 3 and the continuous relaxation

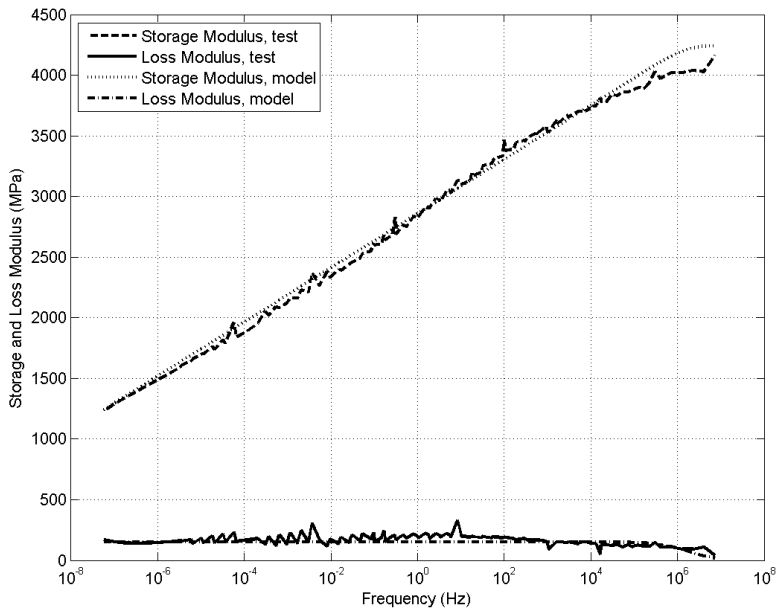


FIG. 3. Comparison between experimental data and constitutive model.

spectrum corresponding to that fit is plotted in Fig. 4. We see that the material behaviour is well-represented by the theory.

In the investigated frequency range between about 10^{-7} Hz and 10^8 Hz, the material behaviour can be adequately represented by the constitutive equations of a viscoelastic fluid. It is not necessary to take an equilibrium stress into account.

The frequency range is fairly large, but in order to investigate and to simulate the long-term creep and relaxation behaviour of PMMA-based bone cement in medical applications, it should be considered that a year has a duration of about 3×10^7 sec and the typical life-time of endoprotheses is about 10–20 years. On the other hand, typical durations of load peaks during sporting activities are about some milliseconds.

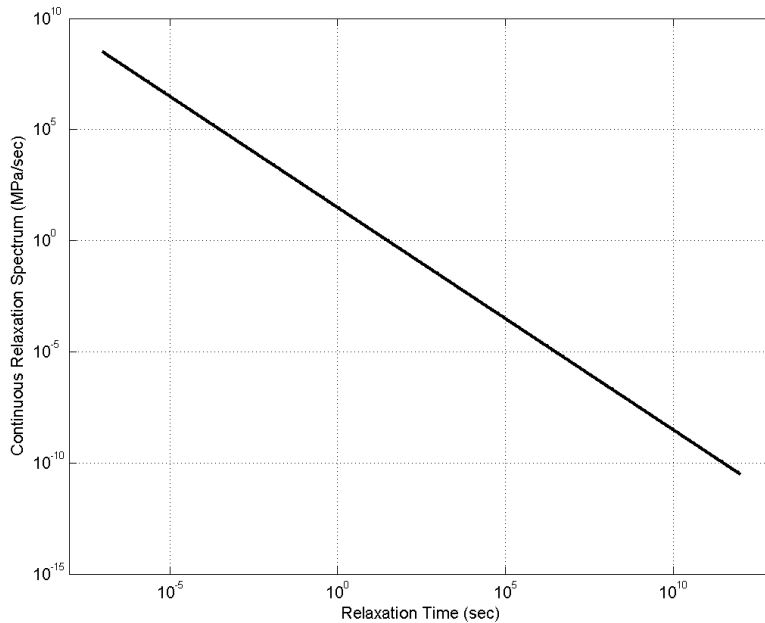


FIG. 4. Continuous relaxation spectrum of PMMA-cement.

Figure 4 shows the continuous relaxation spectrum of PMMA corresponding to the material constants in Tab. 1. Below the relaxation times of 10^{-7} sec and above 10^{12} sec it is identically zero. The short-term tail on the left-hand side of this spectrum is not so essential for applications in medicine: if the duration of a typical shock load occurring during running or jumping is assumed to be about some milliseconds, the shortest relaxation times to be taken into account in the constitutive model should be a factor of ten smaller, i.e. about 10^{-4} sec.

3.4. Approximation of the continuous spectrum

In order to carry out a finite element implementation of this model and/or to make numerical simulations in the time domain, a formulation of the model in terms of ordinary differential equations is very helpful. To this end, we derive a discrete relaxation spectrum whose large number of parameters can be calculated on the basis of the three parameters of the continuous spectrum listed in Tab. 1 and the time range of interest. The corresponding number of differential equations which is necessary to represent the material behaviour depends on the desired accuracy and the dimension of the time range of interest.

Inserting the continuous relaxation spectrum (3.21) into the relaxation function (3.9) we obtain

$$(3.24) \quad G(t) = \mu_0 \int_{z_{\min}}^{z_{\max}} \frac{1}{z} e^{-t/z} dz.$$

It is clear that (3.24) cannot be expressed as the sum of a finite number of decreasing exponentials with good accuracy in the time range $0 \leq t < \infty$. But by HAUPT *et al.* [10] it has been shown that a continuous relaxation spectrum can be approximated within a limited time range

$$(3.25) \quad \tau_{\min} < t < \tau_{\max}$$

by a discrete one. In order to sketch the idea, we substitute in (3.9) the relaxation time by the relaxation frequency $v = 1/z \Leftrightarrow dz = (-1/v^2)dv$ and integrate the result by parts:

$$G(t) = \int_0^{\infty} \left(\frac{h(1/v)}{v^2} \right) e^{-vt} dv = \int_0^{\infty} g(v) e^{-vt} dv = \underbrace{[\Gamma(v) e^{-vt}]_0^{\infty}}_{=0} + t \int_0^{\infty} \Gamma(v) e^{-vt} dv.$$

Based on the cumulative relaxation spectrum $\Gamma(v)$ we obtain the alternative representation

$$G(t) = t \int_0^{\infty} \Gamma(v) e^{-vt} dv \quad \text{with} \quad \Gamma(v) = \int_0^v g(x) dx$$

of the relaxation function. The cumulative spectrum belonging to (3.21) has the form

$$(3.26) \quad \Gamma(v) = \begin{cases} 0 & \text{if } v \leq 1/z_{\max}, \\ \mu_0 \ln(z_{\max} v) & \text{if } 1/z_{\max} \leq v \leq 1/z_{\min}, \\ \mu_0 \ln(z_{\max}/z_{\min}) & \text{if } 1/z_{\min} \leq v. \end{cases}$$

To quantify the lower and upper limits of the time range in which the material behaviour is to be described, the values of τ_{\min} and τ_{\max} in (3.25) have to be specified. With the definitions $v_{\min} = 1/\tau_{\max}$ and $v_{\max} = 1/\tau_{\min}$ the discrete relaxation frequency distribution

$$(3.27) \quad v_k = v_{\min}(v_{\max}/v_{\min})^{(k-1)/(N-1)}$$

required to approximate (3.24) is prescribed. N is the number of exponentials of the Prony series

$$(3.28) \quad G(t) = G_0 + \sum_{k=1}^N G_k e^{-v_k t}.$$

As an estimate, 2–3 exponentials per decade should be taken into account. The moduli G_k in (3.28) are obtained by evaluating the cumulative spectrum (3.26):

$$(3.29) \quad G_0 = \frac{1}{2}(\Gamma(v_1) + \Gamma(v_2)), \quad G_k = \frac{1}{2}(\Gamma(v_{k+1}) - \Gamma(v_{k-1})), \quad 1 \leq k < N.$$

In order to represent the dynamic material behaviour in the whole frequency range, which has been experimentally investigated, we take the choice of $\tau_{\min} = z_{\min}$, $\tau_{\max} = z_{\max}$ and $N = 38$ exponentials. These assumptions lead to the distribution of the moduli G_k as shown in Fig. 5.

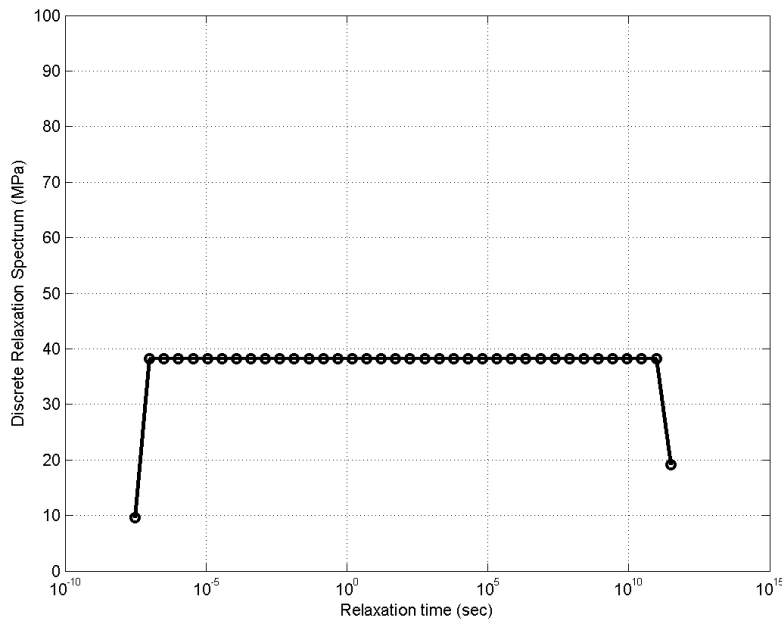


FIG. 5. Elastic moduli of the Prony series with 38 terms: $\tau_{\min} = z_{\min}$, $\tau_{\max} = z_{\max}$.

As we see, the approximation of the continuous relaxation spectrum (3.21) leads to a Prony series with identical values of the moduli G_k , exceptions are only the first and the last ones. It is clear, that such a distribution leads to a nearly frequency-independent loss modulus.

In order to validate this approach and to compare it with the experimental data, we calculate the storage and loss moduli belonging to the Prony series

$$G'(\omega) = 3G_0 + 3 \sum_{k=1}^N G_k \frac{(\omega/v_k)^2}{1 + (\omega/v_k)^2}, \quad G''(\omega) = 3 \sum_{k=1}^N G_k \frac{(\omega/v_k)}{1 + (\omega/v_k)^2}$$

and insert the relaxation frequencies and constants determined by (3.26), (3.27) and (3.29). The results plotted in Fig. 6 show that there is no difference between the dynamic moduli calculated with the continuous spectrum and the discrete one.

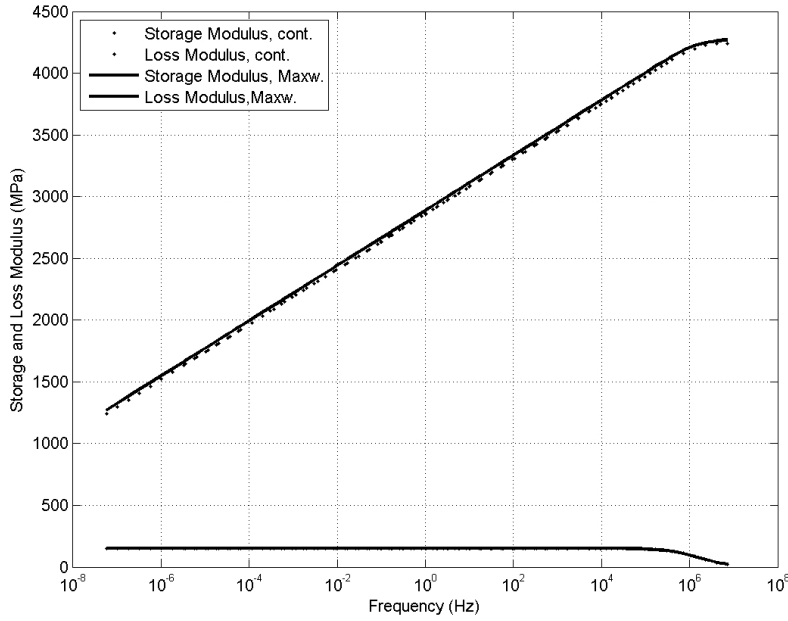


FIG. 6. Moduli of the continuous spectrum and the discrete spectrum with 38 exponentials.

In the case of the discrete relaxation spectrum, the constitutive model can be written as:

$$(3.30) \quad \dot{\mathbf{S}}_k + \frac{1}{\tau_k} \mathbf{S}_k = 2G_k \mathbf{D},$$

$$(3.31) \quad \mathbf{T} = -p\mathbf{1} + G_0 \mathbf{B} + \sum_{k=1}^N \mathbf{S}_k.$$

To represent the viscoelastic material behaviour of PMMA in a limited time range specified by (3.25), the material parameters of (3.30) and (3.31) can be simply calculated with formulae (3.26), (3.27) and (3.29).

Constitutive equations of this type can easily be implemented into in-house finite element codes or are already available in commercial codes and can be used to carry out structural simulations.

3.5. Example

In the case of this example, the time range of interest is assumed to be given by $\tau_{\min} = 0.1$ sec and $\tau_{\max} = 1000$ sec. We take the choice of $N = 12$ exponential terms and calculate the new parameters with formulae (3.26), (3.27) and (3.29). The discrete relaxation spectrum is plotted in Fig. 7 and the corresponding curves of the storage and the loss modulus in Fig. 8. We see, that the discrete model represents the real material behaviour only in a limited frequency range $f_{\min} \leq f \leq f_{\max}$ with $f_{\min} \approx 1/\tau_{\max} = 10^{-3}$ Hz and $f_{\max} \approx 1/\tau_{\min} = 10$ Hz. In order to extend or to reduce this range, a new discrete spectrum has to be determined on the basis of new values for τ_{\min} and τ_{\max} and the formulae (3.26), (3.27) and (3.29).

The method applied in this subsection has shown that the parameters G_k , τ_k and N of the discrete spectrum have no direct physical meaning: they depend

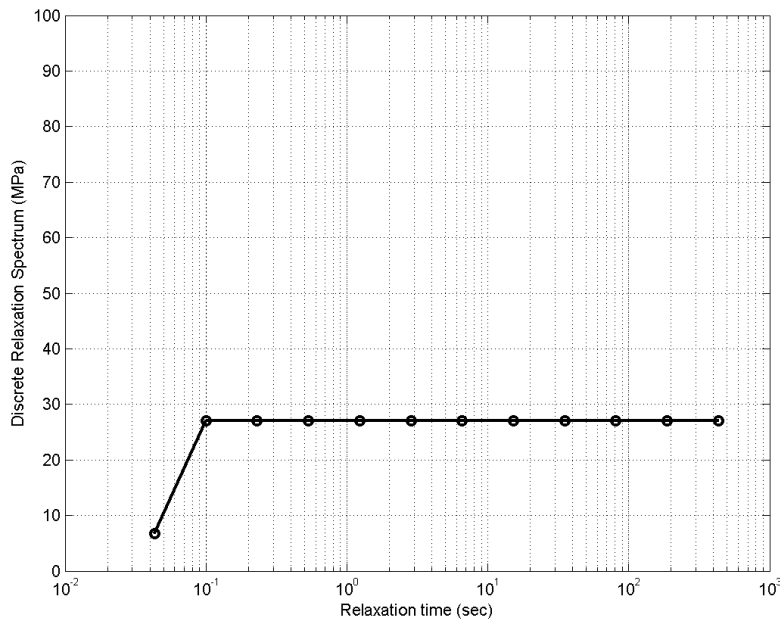


FIG. 7. Elastic moduli of the Prony series with 12 terms: $\tau_{\min} = 0.1$ sec, $\tau_{\max} = 1000$ sec.

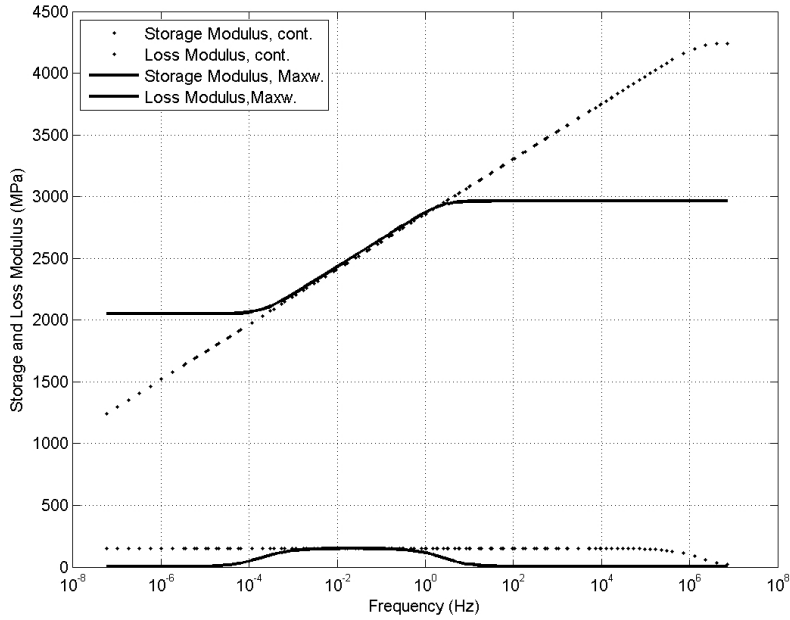


FIG. 8. Moduli of the continuous spectrum and the discrete spectrum with 12 exponentials.

on the frequency or time range where the material behaviour is to be represented. The real parameters of the PMMA-based bone cement are those of the continuous spectrum (3.21), i.e. z_{\min} , z_{\max} and μ_0 .

4. Conclusions

The mechanical behaviour of polymerized PMMA-based bone cement under dynamic strains has been studied with the DMA technique. In the investigated frequency range, the storage modulus is a linear function of the logarithm of the frequency and the loss modulus is nearly constant. This behaviour corresponds to that of a viscoelastic fluid and is manifested by the identified continuous relaxation spectrum which contains no equilibrium modulus. The model has only three material parameters and describes the observed material behaviour with good approximation.

The frequency range considered in this paper is fairly large. But to investigate the long-term behaviour of PMMA-reinforced osteoporotic bones one should consider, that a year has about 3.15×10^7 sec corresponding to a frequency of about 3.17×10^{-8} Hz. The highest frequencies which are caused by short-term loads, for example during sporting activities, are about 10^3 Hz corresponding to characteristic times of 10^{-3} sec. To simulate the material behaviour in such

a known time or frequency range, the approximation method proposed and illustrated in this essay can be successfully applied. In this context, the kernel function of the viscoelastic stress functional, which is determined by a continuous relaxation spectrum, is approximated by a discrete spectrum corresponding to a Prony series with a finite number of terms. The accuracy of this method can be arbitrarily chosen and the $2N + 1$ constants of the Prony series can be calculated using the three parameters of the original continuous spectrum and the dimension of the time range of interest.

The constitutive model developed in this essay is currently implemented into a finite element code. It will be used and further developed in a following project to simulate the short- and long-term behaviour of PMMA-reinforced vertebrae or bone structures. Looking at the theory developed by LION and HÖFER [17], the approach identified in the current work is a fairly important part to represent the thermomechanically-chemically-coupled material behaviour of PMMA in a holistic manner. The most important phenomena to be covered by such a model are the exothermal polymerization, thermal expansion, chemical shrinking and the evolution of residual stresses in curing bone cement. Another very important topic to be studied and constitutively modelled is the diffusion and absorption of salty water in PMMA as well as the corresponding swelling phenomena and changes in the mechanical material properties.

References

1. G. BAROUD, J. NEMES, P.F. HEINI, T. STEFFEN, *Load shift on the intervertebral disc after a vertebroplasty: a finite element study*, Eur. Spine J., **12**, 421–426, 2003.
2. G. BAROUD, M. BOHNER, P.F. HEINI, T. STEFFEN, *Injection biomechanics of bone cements used in vertebroplasty*, Bio-Medical Materials and Engineering, **14**, 487–504, 2004.
3. G. BAROUD, C. VANT, *Long-term effects of vertebroplasty: adjacent vertebral fractures*, Journal of Long-Term Effects of Medical Implants, **15**, 499–514, 2005.
4. G. BAROUD, M. CROOKSHANK, M. BOHNER, *High-viscosity cement significantly enhances uniformity of cement filling in vertebroplasty: an experimental model and study on cement leakage*, Spine, **31**, 2562–2568, 2006.
5. H. BERTILSSON, J.F. JANSSON, *The limits of linear viscoelasticity in Poly-Methyl-Methacrylate and Poly-Ethyl-Methacrylate*, Journal of Applied Polymer Science, **19**, 1971–1978, 1975.
6. G. BÖHME, *Strömungsmechanik nichtnewtonscher Fluide*, Teubner Verlag, 2000.
7. S.V. DOROZHKIN, *Calcium orthophosphate cements for biomedical application*, Journal of Material Science, **43**, 3028–3057, 2008.
8. E.J. HARPER, M. BRADEN, W. BONFIELD, *Mechanical properties of hydroxyapatite reinforced polyethylmethacrylate bone cement after immersion in a physiological solution: influence of a silane coupling agent*, Journal of Materials Science: Materials in Medicine, **11**, 491–497, 2000.

9. P. HAUPT, *Continuum mechanics and theory of materials*, Springer, Berlin 2000.
10. P. HAUPT, A. LION, E. BACKHAUS, *On the dynamic behaviour of polymers under finite strains: constitutive modelling and identification of parameters*, Int. J. Solids Struct., **37**, 3633–3646, 2000.
11. P. HAUPT, A. LION, *On finite linear viscoelasticity of incompressible isotropic materials*, Acta Mechanica, **159**, 87–124, 2002.
12. P.F. HEINI, U. BERLEMANN, M. KAUFMANN, K. LIPPUNER, C. FANKHAUSER, P.V. LANDUYT, *Augmentation of mechanical properties in osteoporotic vertebral bones: a biomechanical investigation of vertebroplasty with different bone cements*, Eur. Spine Journal, **10**, 164–171, 2001.
13. D.G. KIM, M.A. MILLER, K.A. MANN, *Creep dominates tensile fatigue damage of the bone-cement interface*, Journal of Orthopaedic Research, **22**, 633–640, 2004.
14. A.B. LENNON, P.J. PRENDERGAST, *Residual stress due to curing can initiate damage in porous bone cement: experimental and theoretical evidence*, Journal of Biomechanics, **35**, 311–321, 2002.
15. C. LI, S. KOTHA, C.H. HUANG, S. SCHMID, J. MASON, D. YAKIMICKI, M. HAWKINS, *Finite element simulation of thermal behaviour of prosthesis-cement-bone-system*, BED, **50**, Bioengineering Conference, ASME, 235–236, 2001.
16. A. LION, *Thermomechanik von Elastomeren*, Habilitation, Bericht 1/2000, Institute of Mechanics, Faculty of Mechanical Engineering, University of Kassel, 2000.
17. A. LION, P. HÖFER, *On the phenomenological representation of curing phenomena in continuum mechanics*, Archives of Mechanics, **59**, 59–89, 2007.
18. S. MAZZULLO, M. PAOLINI, C. VERDI, *Numerical simulation of thermal bone necrosis during cementation of femoral prosthesis*, Journal of Mathematical Biology, **29**, 475–494, 1991.
19. A. ROHLMANN, T. ZANDER, T. JONY, U. WEBER, G. BERGMANN, *Einfluss der Wirbelkörpersteifigkeit auf den intradiskalen Druck*, Biomed. Technik, **50**, 148–152, 2005.
20. A. ROHLMANN, T. ZANDER, G. BERGMANN, *Spinal loads after osteoporotic vertebral fractures by vertebroplasty of kyphoplasty*, Eur. Spine J., **15**, 1255–1264, 2006.
21. M. STANCZYK, *Study on modelling of PMMA bone cement polymerization*, Journal of Biomechanics, **38**, 1397–1403, 2005.
22. A.V. TOBOLSKY, *Mechanische Eigenschaften und Struktur von Polymeren*, Berliner Union, 1967.
23. N. VERDONSHOT, R. HUISKES, *Dynamic creep behaviour of acrylic bone cement*, Journal of Biomedical Materials Research, **29**, 575–581, 1995.

Received November 14, 2007; revised version May 1, 2008.
